International Journal of Minerals, Metallurgy and Materials
Volume 21, Number 8, August 2014, Page 796
DOI: 10.1007/s12613-014-0973-y

Comparison of TiAlN, AlCrN, and AlCrN/TiAlN coatings for cutting-tool applications

T. Sampath Kumar[1)], *S. Balasivanandha Prabu*[2)], *Geetha Manivasagam*[3)], *and K.A. Padmanabhan*[4)]

1) Department of Mechanical Engineering, C. Abdul Hakeem College of Engineering and Technology, Hakeem Nagar, Melvisharam 632509, India

2) Department of Mechanical Engineering, College of Engineering Guindy, Anna University, Chennai 600025, India

3) School of Mechanical and Building Sciences, VIT University, Vellore 632014, India,

4) School of Engineering Sciences & Technology, University of Hyderabad, Hyderabad 500046, India

(Received: 29 December 2013; revised: 16 March 2014; accepted: 19 March 2014)

Abstract: Monolayer and bilayer coatings of TiAlN, AlCrN, and AlCrN/TiAlN were deposited onto tungsten carbide inserts using the plasma enhanced physical vapor deposition process. The microstructures of the coatings were characterized using scanning electron microscopy (SEM) and atomic force microscopy (AFM). The SEM micrographs revealed that the AlCrN and AlCrN/TiAlN coatings were uniform and highly dense and contained only a limited number of microvoids. The TiAlN coating was non-uniform and highly porous and contained more micro droplets. The hardness and scratch resistance of the specimens were measured using a nanoindentation tester and scratch tester, respectively. Different phases formed in the coatings were analyzed by X-ray diffraction (XRD). The AlCrN/TiAlN coating exhibited a higher hardness (32.75 GPa), a higher Young's modulus (561.97 GPa), and superior scratch resistance (L_{CN} = 46 N) compared to conventional coatings such as TiAlN, AlCrN, and TiN.

Keywords: cutting tools; coatings; physical vapor deposition; characterization; nanoindentation

1. Introduction

To achieve high productivity and precision, nearly 80% of the cutting tools used in manufacturing industries at present utilize hard coatings [1–2]. These hard coatings exhibit very attractive properties, such as high wear resistance and good thermal stability. More recently, nanostructured coatings have been developed that consist of nanocrystalline phases that provide excellent protection to the substrates, even under extreme machining conditions [3]. Several techniques, including physical vapor deposition (PVD) and chemical vapor deposition (CVD), are used to deposit the nanostructured coating over cutting tools. The cathodic arc process is one such PVD technique, where high-ionization-level plasma is used to produce a dense coating [4]. The design of nanostructured coatings depends on various factors, including the crystal size, layer thickness, texture, interface volume, surface, and interfacial energy [5–6]. Compared with TiN coatings, TiAlN, AlCrN, TiCrN, CrN, and TiCN coatings synthesized by the PVD process exhibit improved mechanical properties, such as better oxidation resistance and superior wear resistance [7–8]. The (Ti,Al)N gradient coatings exhibit better qualities, such as the absence of pores and cracks, and high bonding strength [9–10]. Among the coatings developed, TiAlN has been very successful in recent years because of its improved oxidation resistance and hardness compared to those of TiN. In comparison with TiN-based coatings, AlCrN coatings have been reported to exhibit higher oxidation resistance because both chromium and aluminum can form protective oxides, which suppress the diffusion of oxygen. The desired mechanical properties, such as hardness, strength, and Young's modulus of the substrate material, are to be retained when these materials are applied as coatings to extend the use of the cutting tools in extreme machining conditions [11]. Chang *et al.* [10] have reported that TiAlN/CrN coatings exhibit high resistance to plastic deformation and better adhesion strength

Corresponding author: T. Sampath Kumar E-mail: sampatht172@gmail.com

because of the presence of a dense columnar structure. Dobrzański *et al.* [2] have studied various coatings, including Ti/TiN, Ti/TiAlN, Ti/ZrN, TiAl/TiAlN, and Cr/CrN, and analyzed their structure, texture, and chemical composition. The microstructure of the hard PVD coatings exhibits a fine columnar crystallite structure. Therefore, the resultant coatings have exhibited greater strength and hardness. Dobrzański *et al.* [4] have reported that the Ti(B,N) coating exhibits a better adhesion with sintered carbide substrates. The hardness and strength of the coating increased as a result of smaller grains present in the coating.

The literature contains numerous reports on TiAlN coatings combined with TiN, CrN, TiAl, etc. In the present work, the combination of AlCrN and TiAlN coatings was investigated for its application to cutting tools. A cathodic arc vapor deposition (CAVD) process was used to deposit TiAlN, AlCrN, and AlCrN/TiAlN coatings. We then compared the coating characteristics of the TiAlN, AlCrN, and AlCrN/TiAlN materials using scanning electron microscopy (SEM), X-ray diffraction (XRD), nanoindentation, scratch tests and atomic force microscopy (AFM).

2. Experimental

A Balzer's Oerlikon coating machine (Oerlikon Balzers Ltd., India) was used to deposit the coatings. The machine was equipped with eight cathodic arc sources. Four sources (customized sintered targets of Ti) were used to deposit a 0.5 μm-thick TiN sublayer (base coating) over the carbide tool insert. The remaining four sources (50at%Ti–50at%Al customized sintered targets) were used to deposit the TiAlN coating. The eight sources (70at%Al–30at%Cr customized sintered targets) were used to deposit the AlCrN coating. The circular disc-shaped customized sintered targets were placed inside the chamber during the coating process.

The summary of the coating deposition parameters is presented in Table 1. Prior to deposition, all the substrates were cleaned in two steps: first with an ultrasonic pre-cleaner and then with an ultrasonic cleaning machine with 11 tanks, including a hot-air dryer, for 1.5 h. A schematic diagram of the deposition system is illustrated in Fig. 1. Aluminum/chromium or aluminum/titanium materials were placed as targets on the inner sides of the chamber walls to deposit AlCrN and TiAlN coatings, respectively, onto the tool substrate, and a substrate current of 18.5 A was supplied. The argon and N_2 gases were supplied into the chamber, and the gas pressures were maintained on the basis of the chamber pressure.

The temperature of the substrate was measured by a K-type thermocouple positioned near the substrate. The microstructure of the coatings was analyzed using a field-emission scanning electron microscope (FE-SEM) (model SUPRA 55, Germany) equipped with an energy-dispersive X-ray spectroscopy (EDS) apparatus. The phase analysis was conducted using an X-ray diffractometer (model D8–Advance, BRUKER, Germany). The hardness of the coated samples was studied using a nanoindenter (CSM Instruments, Switzerland). The scratch resistance of the coated samples was tested with a Ducom scratch tester, which was equipped with a conically shaped Rockwell C diamond indenter tip; the test were performed according to the standard C 1624–05 (ASTM). The surface morphology of the coated samples was studied using AFM (Nanosurf ® Easy Scan 2 controller, Switzerland).

Table 1. Summary of coating deposition parameters

Argon flow rate / (mL·min^{-1})	800
N_2 flow rate / (mL·min^{-1})	1100
Chamber pressure / Pa	3.2×10^{-2}
Current / A	80
Voltage / V	200
Feed rate for each target / (g·min^{-1})	0.1
Distance between substrate & target / mm	150
Pressure during deposition (Base pressure) / Pa	4.5×10^{-2}
TiAlN coating thickness / μm	4 ± 0.5
AlCrN coating thickness / μm	3 ± 0.5
AlCrN/TiAlN coating thickness / μm	6 ±1
Substrate temperature / °C	450 ± 10
Targets power / kW	7

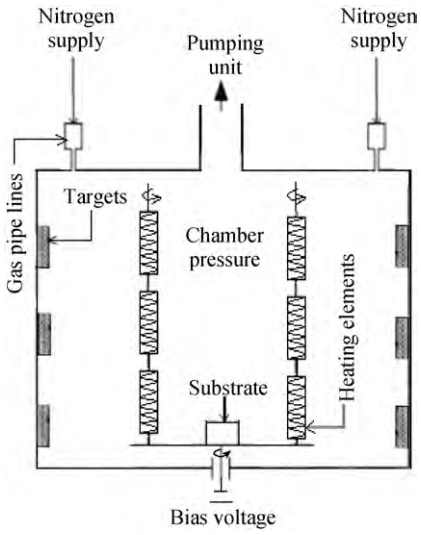

Fig. 1. Schematic diagram of the physical vapor deposition (cathodic arc) system (source diagram: Oerlikon Balzers, Ltd.).

3. Results and discussion

3.1. Microstructural analysis

The EDS spectra and elemental compositions of the TiAlN, AlCrN, and AlCrN/ TiAlN coatings are shown in Figs. 2(a)–2(c), respectively. The cross-sectional and surface views of the TiAlN, AlCrN, and AlCrN/TiAlN coatings over the substrates are shown in Figs. 3(a)–3(c), respectively. The measured thicknesses of the TiAlN, AlCrN, and AlCrN/TiAlN coatings are 4, 3, and 6 μm, respectively. The TiAlN coating exhibits an irregular surface, which is not dense because of the presence of coarse grains.

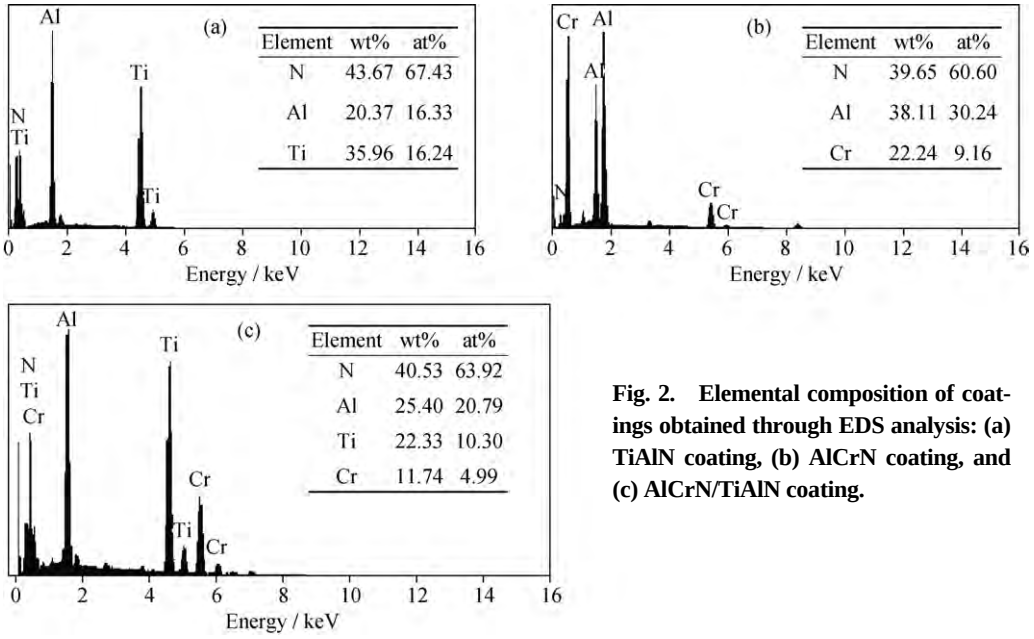

Fig. 2. Elemental composition of coatings obtained through EDS analysis: (a) TiAlN coating, (b) AlCrN coating, and (c) AlCrN/TiAlN coating.

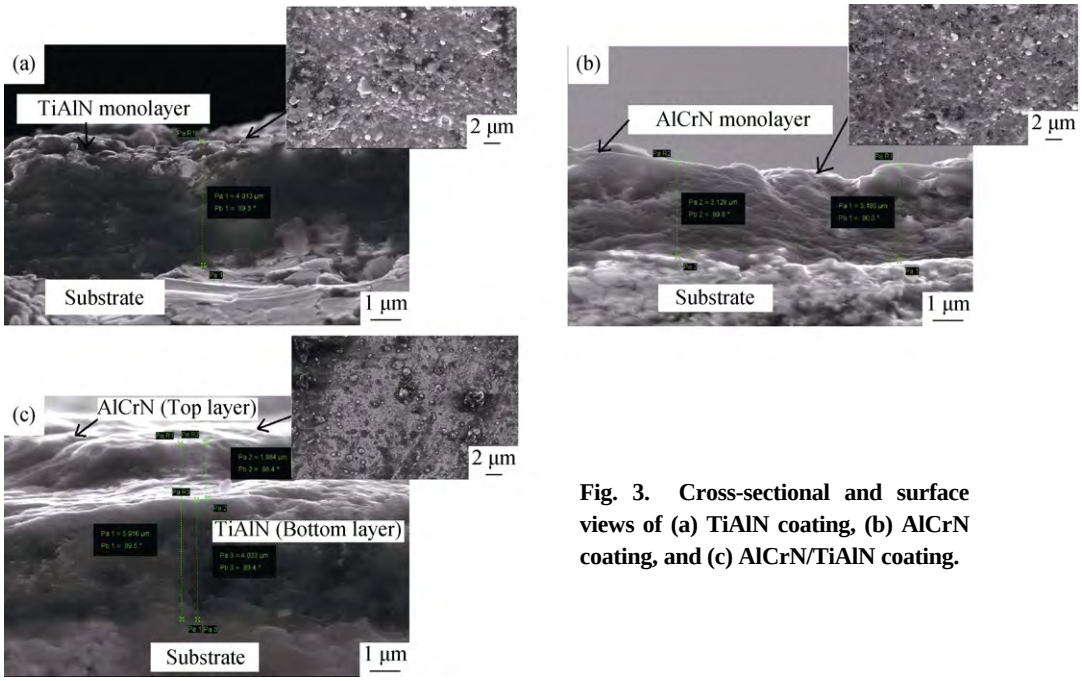

Fig. 3. Cross-sectional and surface views of (a) TiAlN coating, (b) AlCrN coating, and (c) AlCrN/TiAlN coating.

The SEM images in Fig. 3(a) show that the TiAlN layer is bonded perfectly with the substrate. Furthermore, good bonding is observed between the AlCrN and TiAlN layers as a result of interdiffusion. The AlCrN and AlCrN/TiAlN coatings exhibit a regular surface, which is dense because of the presence of fine grains [12–13]. The microstructure shown in Fig. 3(a) clearly indicates that the TiAlN coating contains fewer pores and fewer microvoids because of the

presence of droplets/lumps, which may give rise to a lower hardness value for the coating. Fig. 3(b) and Fig. 3(c) show that the AlCrN and AlCrN/TiAlN coatings exhibit highly dense structures with few pores/microvoids. The interface of the bilayer coating between the AlCrN and TiAlN was not sharp because of interlayer diffusion [14–15].

3.2. XRD analysis

The XRD patterns of the TiAlN, AlCrN, and AlCrN/TiAlN coatings are presented in Figs. 4(a)–4(c), respectively. The scan rate was maintained at 2°/min and the scan range was from 20° to 120°. The XRD patterns confirm that all three different coatings contain phase-pure TiN, CrN, and AlN. The coatings exhibit different patterns for the TiN, AlN, CrN, and TiAlN films with mixed orientations. The intensities of the diffraction peaks gradually decrease with increasing layer thickness, which indicates a gradual decrease in grain size and the weakening of the preferred orientation [16–19].

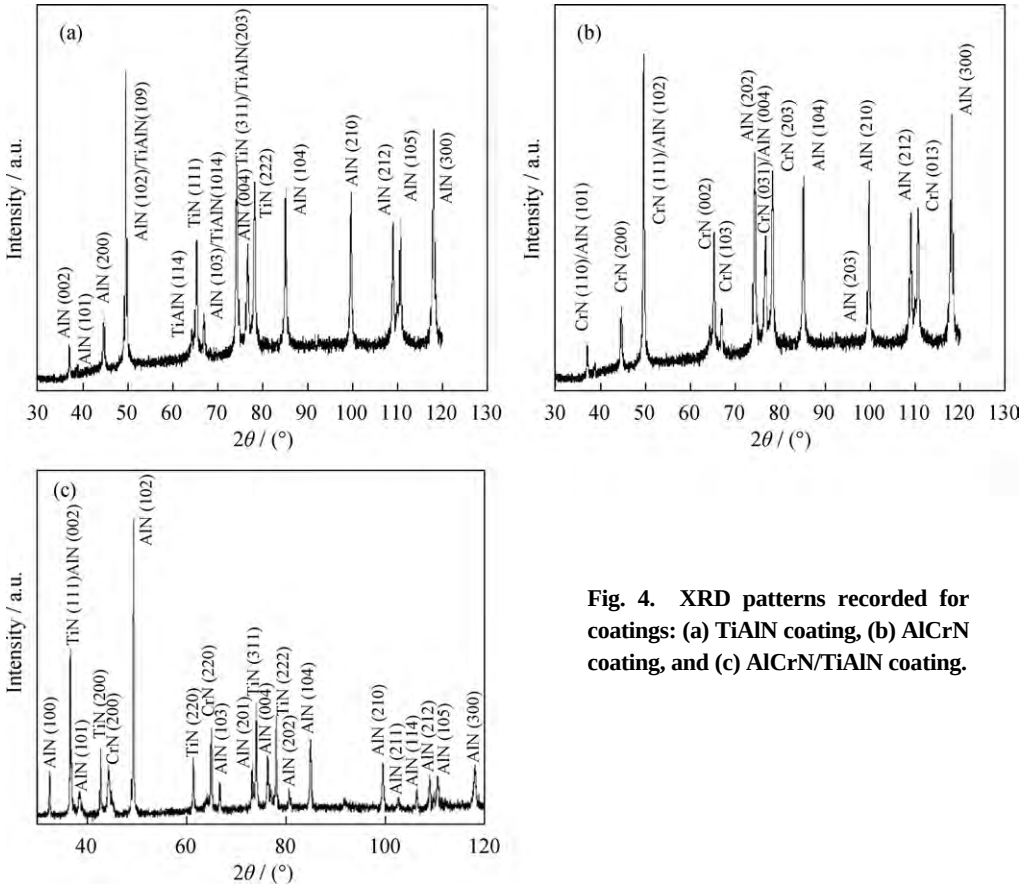

Fig. 4. XRD patterns recorded for coatings: (a) TiAlN coating, (b) AlCrN coating, and (c) AlCrN/TiAlN coating.

The XRD pattern of the TiAlN coating indicates that the AlN (102) and TiAlN (109) planes have a dominant orientation at 49.602° (2θ), as shown in Fig. 4(a). The average crystallite size (D_p), as calculated by the Scherrer equation ($D_p = 0.94\lambda/(\beta\cos\theta)$, where β is the full-width with half-maximum of the peak (in rad), λ is the wavelength of the X-rays (in Å), and θ is the Bragg angle), for the TiAlN coating ranges from 20 to 73 nm. In contrast, in the case of the AlCrN coating, the AlN (102) and CrN (111) planes have a dominant orientation at 49.637° (2θ), as shown in Fig. 4(b). The average crystallite size (D_p) for the AlCrN coating ranges from 24 to 68 nm. In the case of the AlCrN/TiAlN coating, the TiN (111) plane has a dominant orientation, as shown in Fig. 4(c). The TiN peaks indicate a B1–NaCl crystal structure. The sharp peaks in the XRD pattern in Fig. 4(c) indicate a high crystallinity of the AlCrN/TiAlN coating. Fig. 4 also indicates a predominant amount of AlN, followed by TiN and CrN; this result was confirmed by EDS. Because no peak broadening is evident, the grain size of the coating is assumed to be nanocrystalline. We also confirmed that both AlCrN and TiAlN are immiscible because of powder heat of mixing, as indicated by the lack of observed solid solubility. The lack of peak broadening indicates that this process resulted in a strain-free coating. During the initial stage of coating, Al, Ti, and Cr exist in elemental form; as the process progresses, the embedding of Ti particles in Al results in the formation of composite particles. The AlN (102) reflection is intense, and the AlN peaks indicate

(dominant orientation) a wurtzite structure (i.e., B4 hexagonal phase). The CrN (220) plane is the dominant reflection, and the CrN peaks indicate a B1–NaCl crystal structure. The average crystallite size ranges from 30 to 90 nm.

3.3. Nanoindentation tests

The nanoindentation tests were conducted to measure the hardness and the Young's modulus of the coatings. A Berkovich diamond indenter was used to make indentations. The load vs. displacement curves of the TiAlN, AlCrN, and AlCrN/TiAlN coatings are shown in Figs. 5(a)–5(c). The loading/unloading curves show similar responses with respect to stiffness and deformation. The penetration of the Berkovich diamond indenter tip was restricted to less than one-tenth of the coated thickness to preclude any effects of the substrate response. The load was increased after the initial contact of the indenter on the surface at a predetermined rate (100 mN/min) to the desired maximum load (50 mN) and was then decreased at the same rate (100 mN/min) to zero. The measurements of hardness and Young's modulus are mainly based on the unloading curve according to the Oliver and Pharr method [20].

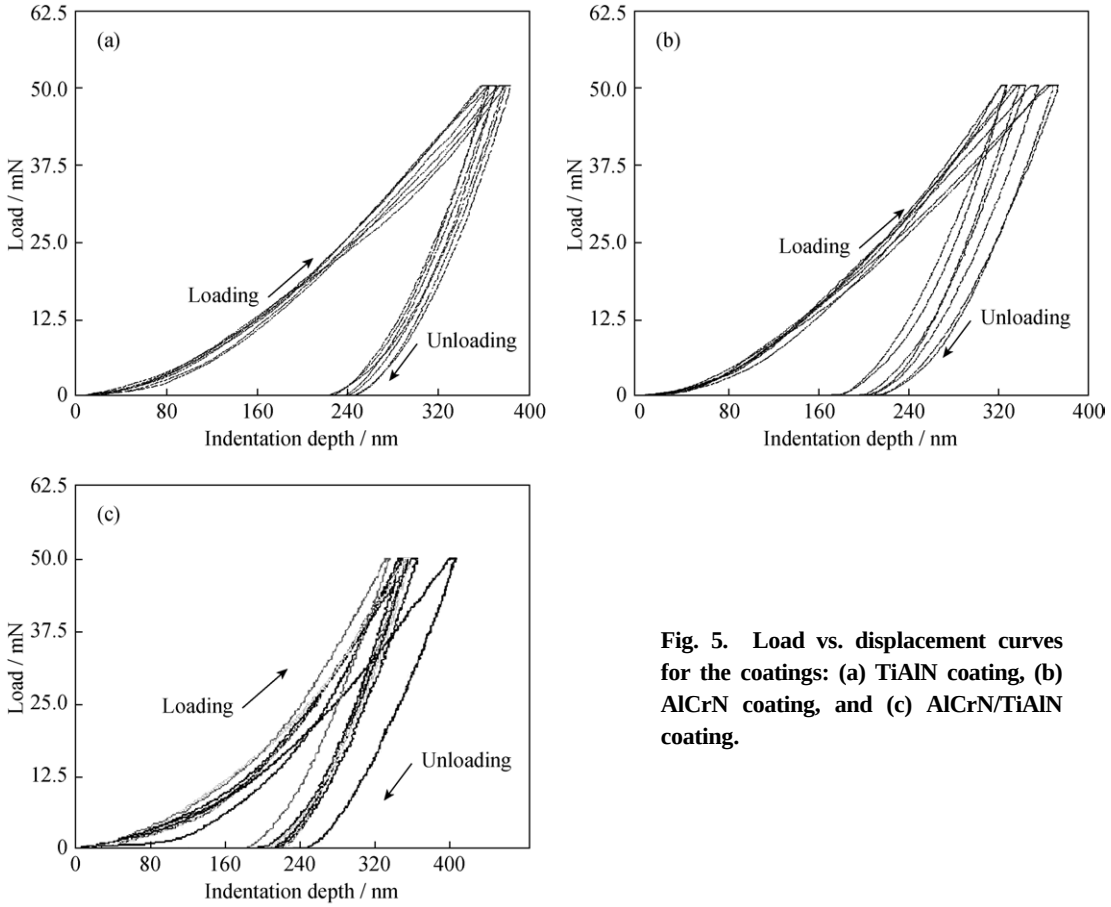

Fig. 5. Load vs. displacement curves for the coatings: (a) TiAlN coating, (b) AlCrN coating, and (c) AlCrN/TiAlN coating.

The TiAlN, AlCrN, and AlCrN/TiAlN-coated samples were subjected to seven trials. The results of their mean values with error bars are given in Table 2. The error bars indicate $a \pm 1$ standard deviation of the mean values. The 99% confidence level (CL) was used to calculate the error bars. The standard deviation values were smaller for all of the mechanical properties of the coating, which indicates that the data points tend to be very close to their mean value. The TiAlN coating exhibited a lower hardness, and the AlCrN coating exhibited a higher hardness, which, however, was less than that of the AlCrN/TiAlN coating. The results clearly indicate that the hardness (H) and Young's modulus (E^*) of the AlCrN/TiAlN coating was higher. A higher value of H^3/E^{*2} indicates high resistance to plastic deformation. Because of the difference in the dense structure and porous nature of the microstructure of the TiAlN, AlCrN, and AlCrN/TiAlN coatings, we obtained different hardness values among the coatings. The elastic recovery (W_e) and plastic recovery (W_p) values were obtained for the AlCrN/TiAlN coating. The mechanical behavior of the coating is understood to strongly depend on its hardness and Young's modulus. The dense structure of the coating leads to higher hardness [21–22].

Table 2. Mechanical properties of coatings calculated from the nanoindentation test for a load of 50 mN

Coating	Hardness, H / GPa	Vickers hardness, HV	Young's modulus / GPa	E^* / GPa	Elastic recovery, W_e / %	Plastic recovery, W_p / %	H^3/E^{*2} / GPa
TiAlN	26.76 ± 0.944	2478.32 ± 87.530	526.45 ± 41.018	578.52 ± 45.075	36.88	63.11	0.0572
AlCrN	31.26 ± 2.782	2914.04 ± 257.740	469.99 ± 75.814	516.47 ± 83.318	48.92	51.07	0.1167
AlCrN/TiAlN	32.75 ± 2.614	3033.015 ± 242.126	561.97 ± 57.620	617.55 ± 58.629	41.34	58.65	0.0921

3.4. Surface morphology

The 3D AFM images of the TiAlN, AlCrN, and AlCrN/TiAlN coatings are presented in Figs. 6(a)–6(c), respectively. The scanner extends the tip along the Z axis to probe for the sample surface. The Z sensor maximum scan range varies from 2 μm to 22 μm. The surface was scanned at a maximum speed of 0.1 mm/s to a range of 10 to 110 μm. The AFM results for surface roughness values are presented in Table 3. The average surface roughness values of the AlCrN/TiAlN bilayer coating was smaller than those of the TiAlN and AlCrN coatings.

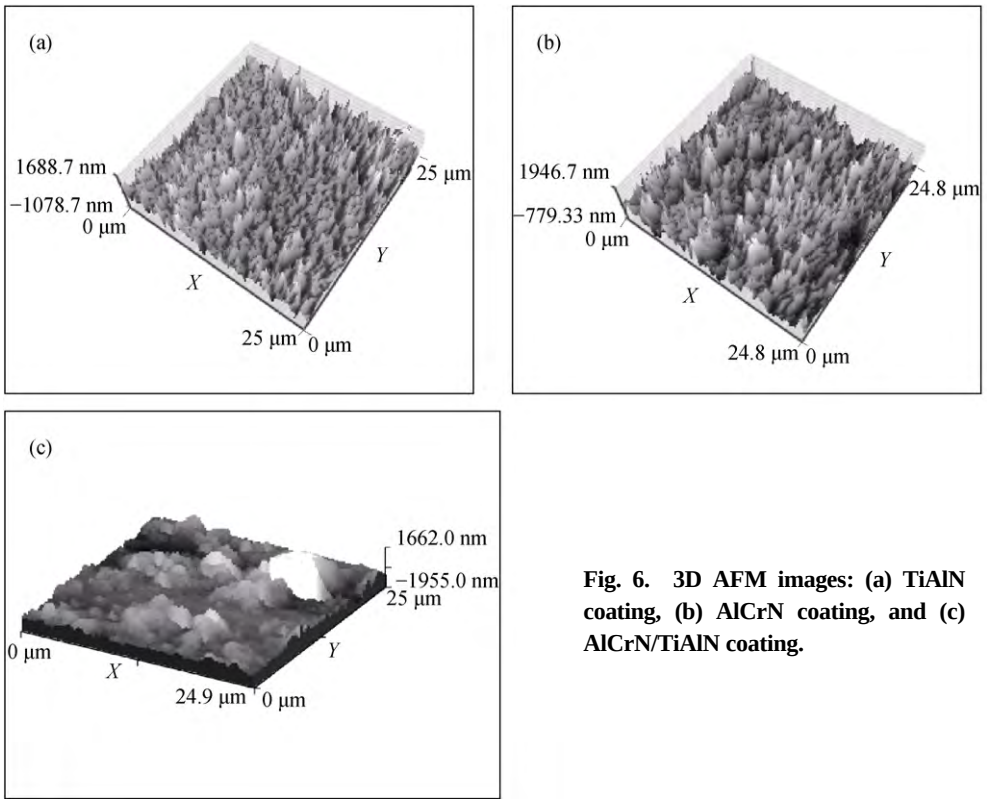

Fig. 6. 3D AFM images: (a) TiAlN coating, (b) AlCrN coating, and (c) AlCrN/TiAlN coating.

Table 3. Surface roughness of coatings, as measured by AFM

Coating	S_a / nm	S_q / nm	S_y / nm	S_p / nm	S_v / nm	S_m / pm
TiAlN	258.20	374.21	2766.8	1688.7	–1078.1	–10.020
AlCrN	255.45	337.58	2726.0	1946.7	–779.33	–10.014
AlCrN/TiAlN	191.00	281.00	3618.0	1662.0	–1955.0	196.00

Note: S_a—roughness, S_q—root mean square, S_y—peak-to-valley height (S_p – S_v), S_p—peak height, S_v—valley depth, and S_m—mean value.

The irregularities of the surface may form nucleation sites for cracks or corrosion, which can be determined using the surface roughness value. A rough surface usually wears more quickly and has a higher friction coefficient than a smooth surface. The waviness observed on a rough surface indicates misorientation of the grains/droplets [23–26]. The surface roughness of the coatings can be increased by improper selection of process parameter values, such as the gas flow rate, the chamber pressure, the current, and the voltage. The TiAlN and AlCrN coatings exhibit surface irregularities and pits; hence, these coatings have higher surface roughness values compared to that of the AlCrN/TiAlN coating. The mixed particle sizes were measured to range from 30 to 582 nm for the TiAlN, AlCrN, and AlCrN/TiAlN coatings.

3.5. Scratch-test analyses

The adhesion and scratch resistance of the coatings were tested using scratch tests. The indenter had a conical tip with a radius of 200 μm and a geometry of 120°. The scratch length was 3 mm, and the scratch speed was 30 mm/min. The loading rate was 300 N/min. The constant loads were 20, 30, 40, and 50 N. The incremental loading rate for the progressive load was 10 N/mm, and the progressive load was 20 N (initial) to 50 N (final). Fig. 7(a), Fig. 8(a), and Fig. 9(a) show the relationship between the traction force and the stroke (length) for the TiAlN, AlCrN, and AlCrN/TiAlN coatings, respectively. The load at which the coating failure occurs is called the critical load (L_{CN}). The traction force and coefficient of friction (μ) can change because of the different types of damage that occur during scratching. These changes can occur as a result of changes in the microstructure, surface roughness along the scratch track, change in the stylus drag, and stress. The uniform dispersion of small particles throughout the substrate causes good adhesion strength. The AlCrN/TiAlN coating exhibited a high critical load of 46.0 N, which indicates that the bonding strength (adhesion strength) of the TiAlN coating with the substrate (base material) is relatively high [27–29].

For the progressive load scratch test, the failure modes of the TiAlN monolayer coating were indicated as L_{C1}, coating cracks (cohesive failure), at 27.5 N; L_{C2}, adhesive chipping at crack edges (adhesive failure), at 32.5 N; L_{C3}, initial failure of the coating, at 36.0 N; and L_{C4}, total failure of the coating, at 41.5 N. For the progressive load scratch test, the failure modes of the AlCrN monolayer coating were indicated as L_{C1}, coating cracks (cohesive failure), at 22.5 N; L_{C2}, adhesive chipping at crack edges (adhesive failure), at 33.0 N; L_{C3}, initial failure of the coating at 42.0 N; and L_{C4}, total failure of the coating, at 45.0 N. For the progressive load scratch test, the failure modes of the AlCrN/TiAlN bilayer

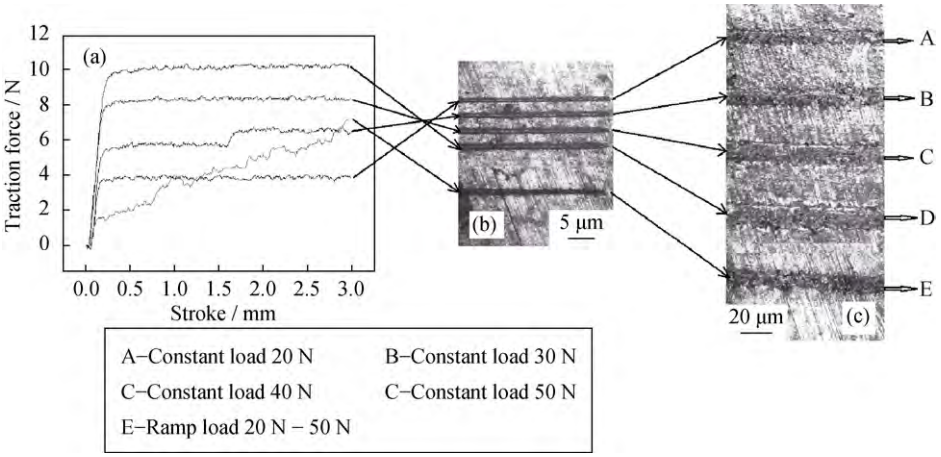

Fig. 7. (a) Traction force vs. stroke curves recorded during a scratch test of the TiAlN coating; (b, c) constant load and progressive load scratch tracks using an optical microscope.

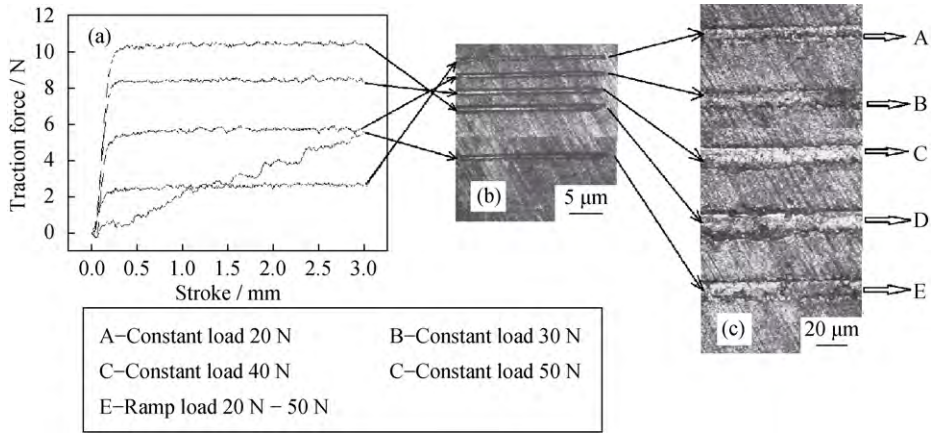

Fig. 8. (a) Traction force vs. stroke curves recorded during a scratch test of the AlCrN coating; (b, c) constant load and progressive load scratch tracks using an optical microscope.

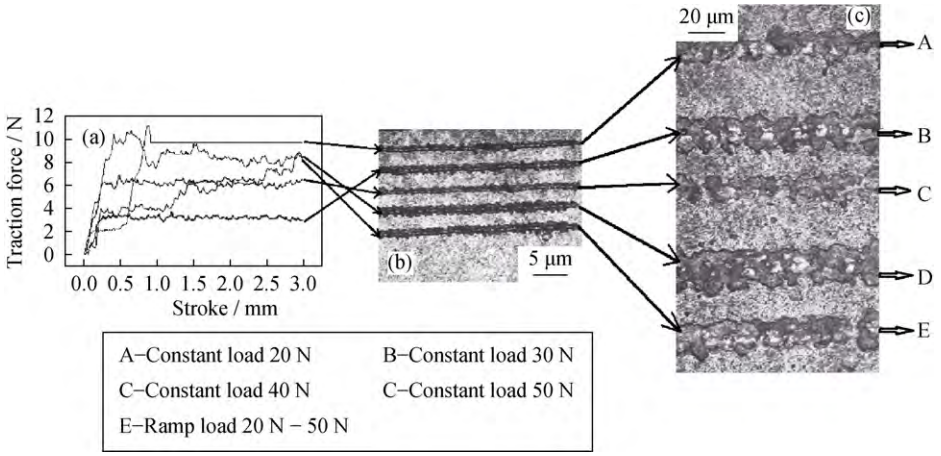

Fig. 9. (a) Traction force vs. stroke curves recorded during a scratch test of the AlCrN/TiAlN coating; (b, c) constant load and progressive load scratch tracks using an optical microscope.

coating were indicated as L_{C1}, coating cracks (cohesive failure), at 21.8 N; L_{C2}, adhesive chipping at crack edges (adhesive failure), at 29.2 N; L_{C3}, initial failure of the coating, at 36.0 N; and L_{C4}, total failure of the coating, at 46.0 N. The values of the failure mode (N) were obtained using Eq. (1), and also the critical load for the progressive type can be calculated by this equation.

$$L_{CN} = \left[L_{rate} \left(I_N / X_{rate} \right) \right] + L_{start} \quad (1)$$

where, L_{rate} is the rate of force application (N/min) in the specific scratch test, I_N is the distance in mm between the start of the scratch track and the starting point of the defined type of damage in the scratch track, X_{rate} is the rate of horizontal displacement (mm/min) in the specific scratch test, and L_{start} is the preload stylus force (N) established at the start of the scratch test.

The optical images of the scratched region of the TiAlN, AlCrN, and AlCrN/TiAlN coatings are shown in Figs. 7(b) and 7(c), Figs. 8(b) and 8(c), and Figs. 9(b) and 9(c), respectively. In the TiAlN and AlCrN monolayer coatings, the splintering of the coatings occurred during the initial stage and the adhesive and delaminating failure occurred because of the increase in the scratch length with respect to time.

In the AlCrN/TiAlN coating, the splintering of the coating occurs in the initial stage because of plastic deformation. However, the splintered coating remains adhered to the substrate. Furthermore, the adhesive failure and delaminating failure occur in the coating because of an increase in the scratch time. The wedging spallation or spalling of the coating occurs in the scratch track because of its ductile nature [30–31]. Furthermore, the adhesive failure occurs in the coating during the second stage (spallation or interface failure). Finally, the coating delaminates, and the total failure of the coating occurs when the scratch time is increased. Thus, the AlCrN/TiAlN bilayer coating has high bonding strength and good scratch resistance, in comparison to the TiAlN and AlCrN monolayer coatings because of its high traction force.

4. Conclusions

TiAlN, AlCrN, and AlCrN/TiAlN coatings were deposited onto tungsten carbide tool substrates using the cathodic arc evaporation process, and the characteristics of the coatings were investigated. The following conclusions are drawn from the test results:

(1) The SEM micrographs show that the AlCrN and AlCrN/TiAlN coatings are denser and have fewer microvoids and microdroplets, which resulted in a uniform structure.

(2) The AFM images show that the AlCrN/TiAlN bilayer coating has low surface roughness (S_a = 191 nm) because it contains fewer macroparticles and fewer surface irregularities. The TiAlN and AlCrN coatings have greater surface roughness values of 258.20 and 255.45 nm, respectively.

(3) The XRD analysis of the deposited bilayer coating shows prominent principal reflections along the (111)/(002) and (102) planes for the AlCrN/TiAlN coating. The crystallite size of the AlCrN/TiAlN coating ranges from 30 to 90 nm.

(4) The nanoindentation test results show that the AlCrN/TiAlN bilayer coating has a hardness of 32.7 GPa and a Young's modulus of 561.97 GPa. The TiAlN coating has a lower hardness of 26.76 GPa and the AlCrN coating has a hardness of 31.26 GPa.

(5) The scratch test results show that the TiAlN, AlCrN, and AlCrN/TiAlN coatings have critical scratch loads (L_{CN}) of 41.5, 45.0, and 46.0 N, respectively, under a progressive load.

Acknowledgements

The authors wish to express their thanks to Oerlikon Balzers Coating India, Ltd. Irrungattukottai, NAL Bangalore and Sathyabama University for providing the facilities to perform these studies and to prepare the manuscript.

References

[1] M. Soković, Quality management in development of hard coatings on cutting tools, *J. Achiev. Mater. Manuf. Eng*., 24(2007), No. 1, p. 421.

[2] L.A. Dobrzański, K. Lukaszkowicz, and K. Labisz, Structure, texture and chemical composition of coatings deposited by PVD techniques, *Arch. Mater. Sci. Eng.*, 37(2009), No. 1, p. 45.

[3] C. Chokwatvikul, S. Larpkiattaworn, S. Surinphong, C. Busabok, and P. Termsuksawad, Effect of nitrogen partial pressure on characteristic and mechanical properties of hard coating TiAlN film, *J. Met., Mater. Miner.*, 21(2011), No. 1, p. 115.

[4] LA. Dobrzański, M. Staszuk, K. Golombek, and M. Pancielejko, Properties of Ti(B,N) coatings deposited onto cemented carbides and sialon tool ceramics, *J. Achiev. Mater. Manuf. Eng.*, 41(2010), No. 1-2, p. 66.

[5] A. Knutsson, M.P. Johansson, L. Karlsson, and M. Odén, Thermally enhanced mechanical properties of arc evaporated $Ti_{0.34}Al_{0.66}N$/TiN multilayer coatings, *J. Appl. Phys.*, 108(2010), art. No. 044312.

[6] A.D. Korotaev, D.P. Borisov, V.Yu. Moshkov, S.V. Ovchinnikov, K.V. Oskomov, Yu.P. Pinzhin, V.M. Savostikov, and A.N. Tymentsev, Nanocomposite and nanostructured superhard Ti–Si–B–N coatings, *Russ. Phys. J.*, 50(2007), No. 10, p. 969.

[7] V. Chawla, A. Chawla, Y. Mehta, D. Puri, S. Prakash, and B.S. Sidhu, Investigation of properties and corrosion behavior of hard TiAlN and AlCrN PVD thin coatings in the 3 wt% NaCl solution, *J. Aust. Ceram. Soc*., 47(2011), No. 1, p. 48.

[8] S. Veprek, S. Mukherjee, H.D. Männling, and J.L. He, On the reliability of the measurements of mechanical properties of superhard coatings, *Mater. Sci. Eng. A*, 340(2003), p. 292.

[9] G. Cabrera, F. Torres, J.C. Caicedo, W. Aperador, C. Amaya, and P. Prieto, Improvement of electrochemical surface properties in steel substrates using a nanostructured CrN/AlN multilayer coating, *J. Mater. Eng. Perform*., 21(2012), p. 128.

[10] Y.Y. Chang, D.Y. Wang, and C.Y. Hung, Structural and mechanical properties of nanolayered TiAlN/CrN coatings synthesized by a cathodic arc deposition process, *Surf. Coat. Technol*., 200(2005), p. 1702.

[11] S. Zhang, D. Sun, Y.Q. Fu, and H.J. Du, Recent advances of superhard nanocomposite coatings: a review, *Surf. Coat. Technol*., 167(2003), p. 113.

[12] G.S. Fox-Rabinovich, K. Yamamoto, M.H. Aguirre, D.G. Cahill, S.C. Veldhuis, A. Biksa, G. Dosbaeva, and L.S. Shuster, Multi-functional nano-multilayered AlTiN/Cu PVD coating for machining of Inconel 718 superalloy, *Surf. Coat. Technol*., 204(2010), p. 2465.

[13] M. Polok-Rubiniec, L.A. Dobrzański, K. Lukaszhowicz, and M. Adamiak, Comparison of the structure, properties and wear resistance of the TiN PVD coatings, *J. Achiev. Mater. Manuf. Eng.*, 27(2008), No. 1, p. 87.

[14] M. Polok-Rubiniec, K. Lukaszhowicz, L.A. Dobrzański, and M. Adamiak, Comparison of the PVD coatings deposited onto hot work tool steel and brass substrates, *J. Achiev. Mater. Manuf. Eng*., 24(2007), No. 2, p. 195.

[15] R. Rebolé, A. Martínez, R. Rodriguez, G.G. Fuentes, E. Spain, N. Watson, J.C. Avelar-Batista, J. Housden, F. Montalá, L.J. Carreras, and T.J. Tate, Microstructural and tribological investigations of CrN coated, wet-stripped and recoated functional substrates used for cutting and forming tools, *Thin Solid Films*, 469-470(2004), p. 466.

[16] M. Polok-Rubiniec, L.A. Dobrzański, and M. Adamiak, Comparison of the PVD coatings, *Arch. Mater. Sci. Eng.*, 38(2009), No. 2, p. 118.

[17] L.A. Dobrzański and L.W. Żukowska, Properties of the multicomponent and gradient PVD coatings, *Arch. Mater. Sci. Eng.*, 28(2007), No. 10, p. 621.

[18] H.C. Barshilia, B. Deepthi, N. Selvakumar, A. Jain, and K.S. Rajam, Nanolayered multilayer coatings of CrN/CrAlN prepared by reactive DC magnetron sputtering, *Appl. Surf. Sci*., 253(2007), p. 5076.

[19] J. Soldán, J. Neidhardt, B. Sartory, R. Kaindl, R. Čerstvý, P.H. Mayrhofer, R. Tessadri, P. Polcik, M. Lechthaler, and C. Mitterer, Structure-property relations of arc-evaporated Al–Cr–Si–N coatings, *Surf. Coat. Technol*., 202(2008), p. 3555.

[20] A.C. Fischer-Cripps, Critical review of analysis and interpretation of nanoindentation test data, *Surf. Coat. Technol*., 200(2006), p. 4153.

[21] J. Musil, F. Kunc, H. Zeman, and H. Poláková, Relationships between hardness, Young's modulus and elastic recovery in hard nanocomposite coatings, *Surf. Coat. Technol*., 154(2002), p. 304.

[22] A. Sivitski, A. Gregor, M. Saarna, P. Kulu, and F. Sergejev, Application of the indentation method for cracking resistance evaluation of hard coatings on tool steels, *Est. J. Eng*., 15(2009), No. 4, p. 309.

[23] S.E. Oraby and A.M. Alaskari, Atomic force microscopy (AFM) topographical surface characterization of multilayer-coated and uncoated carbide inserts, *World Acad. Sci.*

Eng. Technol., 4(2010), p. 396.

[24] M.A. Alaskari, S.E. Oraby, and A.I. Almazrouee, SEM and AFM investigations of surface defects and tool wear of multilayers coated carbide inserts, *World Acad. Sci. Eng. Technol*., 5(2011), p. 530.

[25] H.C. Barshilia, B. Deepthi, K.S. Rajam, K.P. Bhatti, and S. Chaudhary, Growth and characterization of TiAlN/CrAlN superlattices prepared by reactive direct current magnetron sputtering, *J. Vac. Sci. Technol. A*, 27(2009), p. 29.

[26] P.V. Zinin, V.L. Solozhenko, A.J. Malkin, and L.C. Ming, Atomic force microscopy studies of cubic BC_2N, a new superhard phase, *J. Mater. Sci.*, 40(2005), p. 3009.

[27] B. Warcholinski and A. Gilewicz, Tribological properties of CrN_x coatings, *J. Achiev. Mater. Manuf. Eng*., 37(2009), No. 2, p. 498.

[28] M. Hagarová, I. Štěpánek, and D. Jakubéczyová, Evaluation of thin PVD coatings by adhesive–cohesive test, *Acta Metall. Slovaca*, 16(2010), No. 3, p. 157.

[29] W. Pawlak and B. Wendler, Multilayer, hybrid PVD coatings on Ti6Al4V titanium alloy, *J. Achiev. Mater. Manuf. Eng.*, 37(2009), No.2, p. 660.

[30] X.L. Pang, K.W. Gao, F. Luo, Y. Emirov, A.A. Levin, and A.A.Volinsky, Investigation of microstructure and mechanical properties of multi-layer Cr/Cr_2O_3 coatings, *Thin Solid Films*, 517(2009), p. 1922.

[31] LA. Dobrzański, S. Skrzypek, D. Pakula, J. Mikula, and A. Kříž, Influence of the PVD and CVD technologies on the residual macro stresses and functional properties of the coated tool ceramics, *J. Achiev. Mater. Manuf. Eng*., 35(2009), No. 2, p. 162.